



ELSEVIER

## Gamma-ray energy determination using neural network algorithms for an imaging silicon calorimeter

R. Borisjuk<sup>a</sup>, M. Casolino<sup>b</sup>, M.P. De Pascale<sup>b</sup>, A. Morselli<sup>b</sup>, P. Picozza<sup>b</sup>, A. Ogurtsov<sup>a</sup>,  
M. Ricci<sup>c</sup>, R. Sparvoli<sup>b,\*</sup>

<sup>a</sup>*Institute of Mathematical Problems of Biology, Russian Academy of Sciences, Pushchino, Russian Federation*

<sup>b</sup>*Department of Physics, II University of Rome "Tor Vergata" and INFN, Sec. Roma II, Roma, Italy*

<sup>c</sup>*INFN Laboratori Nazionali di Frascati, Frascati, Italy*

Received 15 April 1996

### Abstract

A neural network technique, based on multi-layer perceptrons, is used to fully exploit the performances of a sampling silicon calorimeter in energy identification of gamma rays. The results obtained on simulated data are significantly better than those coming from a classic method analysis.

### 1. Introduction

The WiZard collaboration has been devoted to the research of primary antimatter in cosmic radiation since 1989. This activity has been carried on by stratospheric balloon launches from American (Fort Sumner) and Canadian (Prince Albert, Lynn Lake) bases [1,2]. The instrumentation flying on balloons is constituted by a magnetic spectrometer (a superconducting magnet with a tracking system), a  $\beta$  selector (Cherenkov counter or TRD or RICH), a time of flight system and an electromagnetic calorimeter. The present calorimeter [3,4] consists of active silicon strip layers interleaved with passive planes made of a showering high Z material (tungsten). Tests on a prototype of the calorimeter which took place at CERN [5] have shown that such a device could reach good performances even in detection of  $\gamma$  rays with energy greater than 20 MeV (pair production regime), both in energy and in angular resolution. Since then, detailed simulations in order to find an optimised set-up for a gamma telescope have started. The GILDA detector, described in the next section, is a product of such analysis.

The activity of the WiZard collaboration will be extended in the future by three satellite missions joined in the RIM (Russian–Italian Mission) program: NINA, interested in low energy cosmic ray observations, PAMELA, devoted to antimatter observations as a natural extension of the balloon activity, and GILDA, dedicated to the detection of high energy gamma radiation.

High energy gamma-ray astrophysics has greatly developed in these last few years thanks to the results of the experiment EGRET [6,7], on the Compton Gamma Ray Observatory. The satellite observations have brought more detailed data about the known gamma-ray sources, but also the discovery of new sources, both galactic and extragalactic, especially active galactic nuclei and gamma-ray bursts. Nevertheless, the emission mechanisms of these sources are not yet clear so that the investigation of the high energy component of the cosmic gamma radiation with a telescope working in a energy interval broader than EGRET is of crucial importance.

The upper part of EGRET apparatus consists of spark chambers that allow the conversion of the  $\gamma$  rays in electron–positron pairs and the identification of their tracks for source pointing. The lower part is made of a NaI(Tl) crystal where the development of the shower takes place and most part of the initial energy is deposited.

A strong limitation of the EGRET instrument is due to the spark chambers. They need periodic substitutions of the filling gas to work properly and this requirement causes weight and duration time problems for a space experiment. Moreover they have quite a long dead time, especially if related to the typical length of transient phenomena like gamma ray bursts. Finally, the track resolution of such detectors is not better than a few millimeters.

These problems can be overcome with the adoption of silicon strip detectors. The silicon technology for cosmic ray research, especially for gamma ray astrophysics, is being adopted by other collaborations too [8], since it ensures a net improvement in source pointing with respect to gas detectors. On the other hand, the GILDA detector

\* Corresponding author. Tel. +39 6 72594513, fax +39 6 2025364, E-mail sparvoli@roma2.infn.it.

being a sampling silicon calorimeter, the energy resolution depends directly on the thickness of the passive material interposed. The energy resolution for this kind of detector can be improved by increasing the number of active silicon layers; however, in space missions a limited weight is a very strong requirement and therefore the adoption of new and more powerful algorithms, besides the classic ones, able to improve the energy resolution performances of the next generation  $\gamma$  telescopes is highly recommended. The neural network technique could be a good solution, as it will be shown in the following sections; several algorithms of pattern recognition, based on neural networks, have already been developed by the WiZard collaboration [9,10].

## 2. The GILDA imaging calorimeter

The core of the GILDA telescope is a space version of the calorimeter presently used in the WiZard program balloon flights, based on the use of silicon strip fine-grained detectors. The basic element is a  $6 \times 6 \text{ cm}^2$  module, shown in Fig. 1, composed by two Si-D detectors (SI-D), each  $380 \mu\text{m}$  thick and mounted back to back with perpendicular strips in order to give the  $X$  and  $Y$  coordinates. Each module has  $16 \times 2$  strips,  $3.6 \text{ mm}$  wide [11].

The GILDA calorimeter in its baseline configuration is a stack of 20 planes, each one composed by 64 Si-D modules already described and  $50 \times 50 \text{ cm}^2$  wide. The stratigraphy of the calorimeter is shown in Fig. 2. The structure is divided in two sections: the first ten planes have the silicon layers, except the upper two, interleaved with tungsten plates of  $0.15 X_0$  thickness; this part provides source pointing for low energy gamma rays. The last ten planes, instead, have  $1 X_0$  thick tungsten plates between each pair. In between, a  $2 \text{ cm}$  aluminium layer is interposed: the whole calorimeter is then  $11.73 X_0$  thick. Finally, anticoincidence plastic scintillators  $A_c$  and  $A_s$  are placed around the upper zone in order to reject charged particles.

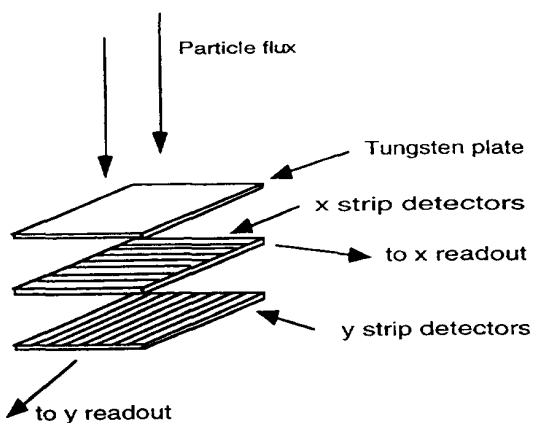


Fig. 1. A diagram of the  $6 \times 6 \text{ cm}^2$  double-sided silicon wafer.

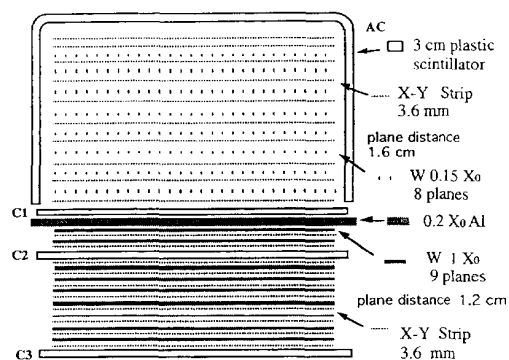


Fig. 2. Stratigraphy of the GILDA calorimeter.

tillators  $A_c$  and  $A_s$  are placed around the upper zone in order to reject charged particles.

Other configurations of GILDA telescope have already been studied; further details on this instrument can be found in Refs. [12,13].

In GILDA calorimeter, the gamma ray energy is measured through the electromagnetic cascade by means of the signals released in the silicon strips. However, due to the weight limitations, only a part of the shower can be detected. Indeed, 98% of the shower at  $1 \text{ GeV}$  is contained in a thickness of approximately  $21 X_0$ , much bigger than the length of the whole GILDA calorimeter ( $11.73 X_0$ ).

## 3. Gamma energy determination

### 3.1. Simulations and data filtering

Data have been simulated in the energy interval from  $100 \text{ MeV}$  to  $90 \text{ GeV}$  using the GEANT 3.15 code [14]. Photons (a sample of 1000 events for each energy) hit the calorimeter orthogonally, at the center of the first plane. Fig. 3 shows the behavior of a simulated gamma ray interaction in the calorimeter at different energies. As a result of a number of optimisations, an energy cut has been fixed at  $10 \text{ keV}$ ; this means that GEANT follows a secondary particle until its energy is above or equal this value, then departs this energy at this point. For each active strip, a threshold corresponding to an energy of  $0.5 \text{ mips}$  (minimum ionising particle) has been imposed to reproduce the experimental situation and, indeed, to eliminate the noise of the electronics from the data. During the tests made at CERN with the prototype of the WiZard calorimeter, the reliability of the Monte Carlo simulations, based on the same code, in reproducing real events has been checked; an excellent agreement between real and simulated data has been obtained [5].

The development of the shower and the connected energy released in the calorimeter depend strongly on the conversion point of the primary gamma-ray: there is no

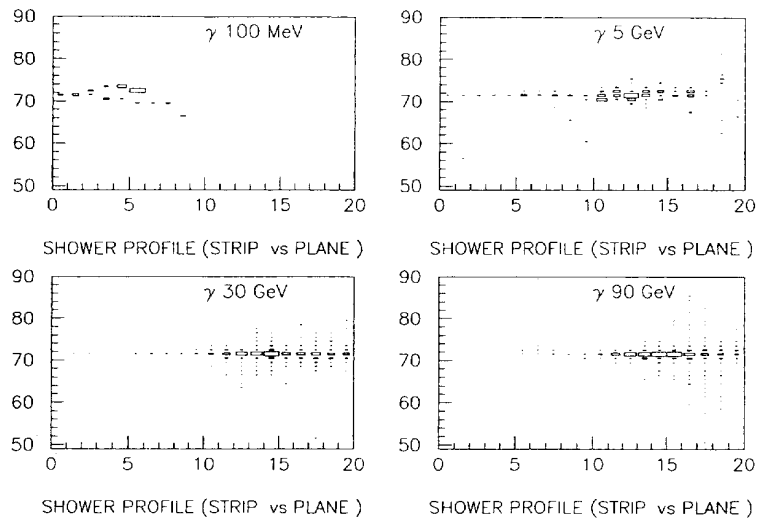


Fig. 3. Energy released in the calorimeter for simulated gammas at different energies.

signal before its conversion to an electron–positron pair. In our analysis, in order to get a reliable estimation of the gamma initial energy, we request the shower maximum to be contained in the calorimeter; therefore the following filter to the input data has to be applied:

- 1) The maximum of the shower must, for each event, be in one of the planes of the calorimeter, except the last.
- 2) Strips must be hit in at least 3 planes (6 views), important request for low energy events.

The number of data lost because of this choice is energy-dependent and has been reported in Table 1 for a few energies.

### 3.2. Classic algorithm

We started reconstructing the gamma energy by a classic algorithm. A gamma-ray interacts in the GILDA calorimeter and produces an electromagnetic shower. The number of secondaries produced is proportional to the incoming particle energy and so this one will be linearly related to

the sum  $E_{\text{tot}}$  of the energies  $e_{i,p}$  released by the shower particles in the  $N_{\text{strip}}$  strips of the  $N_{\text{plane}}$  planes of the calorimeter:

$$E_{\text{tot}} = \sum_{i=1, p=1}^{N_{\text{strip}}, N_{\text{plane}}} e_{i,p}. \quad (1)$$

From this value we can derive the initial gamma energy.

To establish the energy resolution  $R$  of our apparatus we constructed, for each sample of simulated events, the distribution function of  $E_{\text{tot}}$  and, then, operated a Gaussian fit.  $R$  is defined as the ratio between the sigma and the mean value of the Gaussian distribution. Results obtained for the explored energies are shown in Fig. 5.

In this analysis only one discriminating parameter was used and the development of the shower in the calorimeter was not considered. To improve the results, other discriminating parameters should be added and their relationships taken into account using logical operators and fixed boundaries. This procedure, however, leads to an important loss of efficiency due to the overlapping of the distribution functions of these parameters for different energies.

### 3.3. Neural networks

If neural networks (NN) are used to determine a gamma-ray energy, it is possible to automatically take into account some information coming from several discriminating parameters without needing to resort to a discrete logic decision tree. It is also possible to exploit typical advantages of the NN such as automatic learning process, extraction of useful information from examples, noise resistance, parallelity of computations.

Table 1  
Percentage of loss of events using the input selection filter

Energy of gamma [MeV]	Percentage of dropped events
100	39.0
500	5.4
1000	1.7
2000	1.5
3000	1.8
5000	2.4
10 000	3.2
50 000	8.0
90 000	8.0

3.3.1. Architecture

The primary gamma energy range we are able to study with GILDA detector extends over several orders of magnitude (100 MeV–90 GeV); therefore we have opted for a two step net architecture, shown in Fig. 4. In the first stage, a net performs a rough classification of the gamma energies in six groups. Then, for each group, a dedicate net proceeds to discriminate among the different energy values. As in the classic phase, we used simulated data sets to train and test the NN.

The net employed in the first stage is a Multi-Layer Perceptron (MLP), consisting of 7 input neurons (the discriminating parameters), 6 output neurons (the classes) and two hidden layers, each with 10 neurons. The output neuron with the highest activation value has been used for the classification. The training has been performed dividing the energy interval in six classes.

At the second stage we have used six MLPs; each MLP determinates the energy value of the corresponding subclass. The output layer consists of  $N_{oi}$  nodes equal to the number of the different energy subclasses used in the training phase. This way the net has a discrete output and

is able to classify only those energies used during training. Since gamma rays have a continuous energy distribution, the following weighted average over the output neurons value has been performed:

$$E_\gamma = \frac{\sum_{i=1}^{N_{oi}} o_i e_i}{\sum_{i=1}^{N_{oi}} o_i}, \quad (2)$$

where  $e_i$  is the energy corresponding to gamma rays of class  $i$  and  $o_i$  is the activation value of the output neuron  $i$ .

This way, the classification is not performed on a “winner takes all” basis, but on a “common agreement” one. Comparative results have shown that the discrimination capability of the architecture is better than that of a net with only one continuous output neuron, for which there is a proportional relation between its activation value and the energy of the primary gamma ray (in this case no sigmoid function was used on the output neuron and the learning value was modified accordingly).

For training, the classes were divided, within the intervals defined in the first stage, in subclasses with the following energy values:

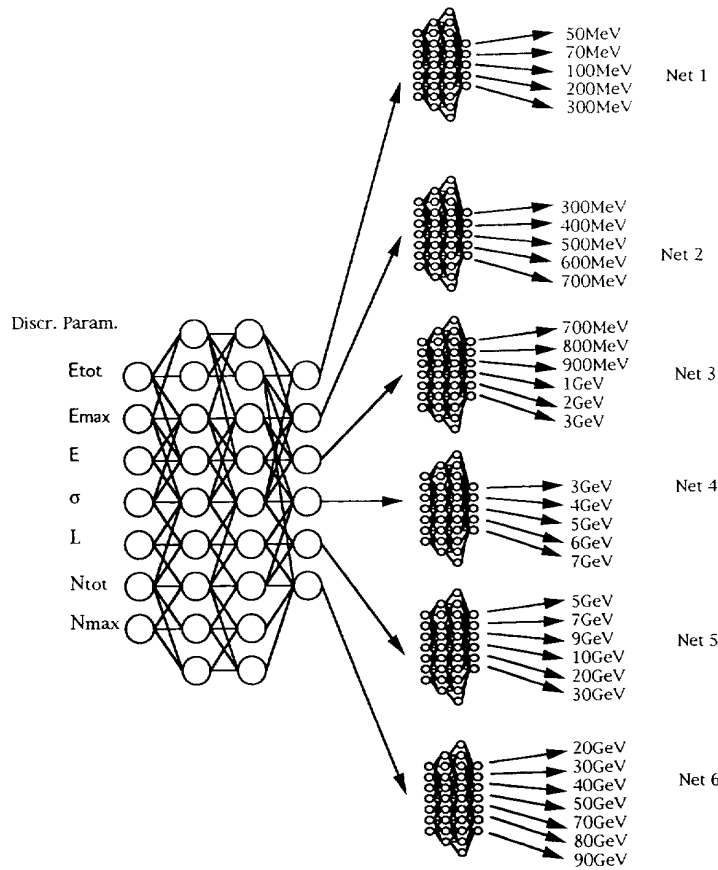


Fig. 4. Flow chart of the neural network analysis algorithm.

- Net 1: 50, 70, 100, 200, 300 MeV;  $N_o = 5$ ;
- Net 2: 300, 400, 500, 600, 700 MeV;  $N_o = 5$ ;
- Net 3: 700, 800, 900, 1000, 2000, 3000 MeV;  $N_o = 6$ ;
- Net 4: 3000, 4000, 5000, 6000, 7000 MeV;  $N_o = 5$ ;
- Net 5: 5000, 7000, 9000, 10 000, 20 000, 30 000 MeV;  $N_o = 6$ ;
- Net 6: 20 000, 30 000, 40 000, 50 000, 70 000, 80 000, 90 000 MeV;  $N_o = 7$ .

One or two highest energies in each group were included also in the subsequent net in order to avoid boundary effects. We used two hidden layers with 71 and 21 neurons (71 × 21 configuration) for nets 1 and 2 respectively, a 60 × 20 configuration for nets 3 and 4, and finally, for the last two nets (net 5 and 6), a 20 × 15 configuration.

### 3.3.2. Discriminating parameters

The input layer of each MLP contains 7 neurons related to 7 discriminating parameters. The gamma ray may convert at any point in the calorimeter, so that the signal released may substantially differ even for the events meeting the condition of maximum of energy detected. Thus, we used parameters as much as possible independent from the conversion point, such as the following ones:

- 1)  $E_{\text{tot}} = \sum_{i=1, p=1}^{N_{\text{strip}}, N_{\text{plane}}} e_{i,p}$ , total energy released in the calorimeter.
- 2)  $E_{\text{max}} = E(p_{\text{max}})$ , energy released in the plane with the maximum deposit ( $p_{\text{max}}$ ).
- 3)  $E = \sum_{i=1, p=1}^{N_{\text{strip}}, p_{\text{max}}} e_{i,p}$ , sum of the energy released up to the plane of maximum deposit.
- 4)  $\sigma = \sqrt{\sum_{i=1}^{N_{\text{strip}}} e_{i,p} (x_i - \bar{x}_p)^2 / E_p}$ , lateral spread of the shower, being  $x_i$  the strip counter ( $1 \leq x_i \leq 128$ ),  $E_p$  the total energy released in plane  $p$  and  $\bar{x}_p = \sum_{i=1}^{N_{\text{strip}}} e_{i,p} x_i / E_p$ .
- 5)  $L = p_{\text{max}} - p_{\text{conversion}}$ , “length” of the shower from the conversion plane to the one of maximum deposit.
- 6)  $N_{\text{tot}} = \sum_{i=1, p=1}^{N_{\text{strip}}, N_{\text{plane}}} y_{i,p}$ , total number of hit strips in the calorimeter, being

$$y_{i,p} = \begin{cases} 1 & e_{i,p} > 0, \\ 0 & \text{otherwise.} \end{cases}$$

7)  $N_{\text{max}} = \sum_{i=1, p=1}^{N_{\text{strip}}, p_{\text{max}}} y_{i,p}$ , number of hit strips up to the plane of maximum deposit.

### 3.3.3. Results

The gamma energies have been determined summing all the activated neurons with their appropriate weights; the mean value and the sigma, as in the classic case, were evaluated by the distributions of the simulated data samples. For boundary energies, the weighted sums of the reconstructed energies and sigmas from the two overlapping classes have been made. The results obtained with the NN algorithm are shown in Fig. 5 together with those coming from the classic analysis. The flatness of the energy resolution at high energies, evident for both the algorithms, is related to the longitudinal leakage of the shower. In the interval explored, the improvement obtained in the energy resolution by using neural networks ranges from 20% to 40%.

The method appears to be really effective for energies up to 1 GeV, for which this kind of calorimeter has a rather poor energy resolution.

## 4. Conclusions

An analysis performed on simulated samples of gamma rays impinging on a silicon–tungsten imaging calorimeter, by using a neural network architecture employing multi-layer perceptrons, results in an energy determination significantly improved if compared to classic methods.

## References

- [1] R.L. Golden et al., Nuovo Cimeno B 105 2 (1990) 191.
- [2] G. Barbiellini et al., Nuovo Cimento B 102 (1988) 661.
- [3] F. Aversa et al., Nucl. Instr. and Meth. A 360 (1995) 17.
- [4] M. Bocciolini et al., Nucl. Instr. and Meth. A 370 (1996) 403.
- [5] M. Bocciolini et al., Nucl. Instr. and Meth. A 333 (1993) 560.
- [6] G. Kanbach et al., Space Sci. Rev. 49 (1988) 69.
- [7] C. Fichtel et al., Astrophys. J. Suppl. 94 (1994) 551.
- [8] W.B. Atwood et al., Nucl. Instr. and Meth. A 342 (1994) 302.
- [9] M. Candusso et al., Nucl. Instr. and Meth. A 360 (1995) 371.
- [10] F. Aversa et al., Astroparticle Phys. 5 (1996) 111.
- [11] M. Bocciolini et al., Nucl. Phys. B 32 (1993) 77.
- [12] G. Barbiellini et al., Nucl. Instr. and Meth. A 354 (1995) 547.
- [13] G. Barbiellini et al., Nucl. Phys. B 43 (1995) 253.
- [14] R. Brun et al., CERN GEANT 3 User’s guide, DD/EE/84-1 (1992).

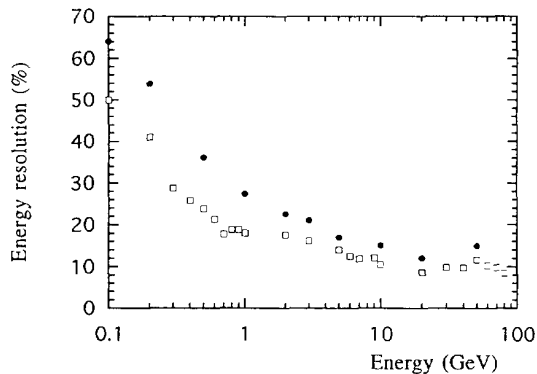


Fig. 5. Energy resolution (%) versus energy of the primary particle (GeV); bullets: classic algorithm; squares: neural network.